Ultra-high flux alkali-treated cellulose triacetate/cellulose nanocrystal nanocomposite membrane for pervaporation desalination

by Indah Prihatiningtyas

Submission date: 17-Mar-2022 11:57AM (UTC+0700)
Submission ID: 1786144802
File name: alkaline_treatment.pdf (1.17M)
Word count: 6720
Character count: 35241

ARTICLE IN PRESS

Chemical Engineering Science xxx (xxxx) xxx

Contents lists available at ScienceDirect

Chemical Engineering Science

journal homepage: www.elsevier.com/locate/ces

Ultra-high flux alkali-treated cellulose triacetate/cellulose nanocrystal nanocomposite membrane for pervaporation desalination

Indah Prihatiningtyas [a,b,*], Yusak Hartanto [c], Bart Van der Bruggen [a,d,*]

[a] Department of Chemical Engineering, KU Leuven, Celestijnenlaan 200F, B-3001 Leuven, Belgium
[b] Department of Chemical Engineering, Mulawarman University, Jalan Sambaliung No.9, Sempaja Selatan, Samarinda, Kalimantan Timur, Indonesia
[c] Materials and Process Engineering (iMMC-IMAP), UC Louvain, Place Sainte Barbe 2, 1348 Louvain-la-Neuve, Belgium
[d] Faculty of Engineering and the Built Environment, Tshwane University of Technology, Private Bag X680, Pretoria 0001, South Africa

HIGHLIGHTS

- Alkaline post-treatment significantly boosted the hydrophilicity of CTA/CNCs membranes.
- Alkaline post-treatment enhanced the performance of CTA/CNCs membranes.
- 30 min is the optimum time for alkaline treatment of CTA/CNCs membranes.
- Alkali-treated membrane was able to handle highly saline water without losing its selectivity.

GRAPHICAL ABSTRACT

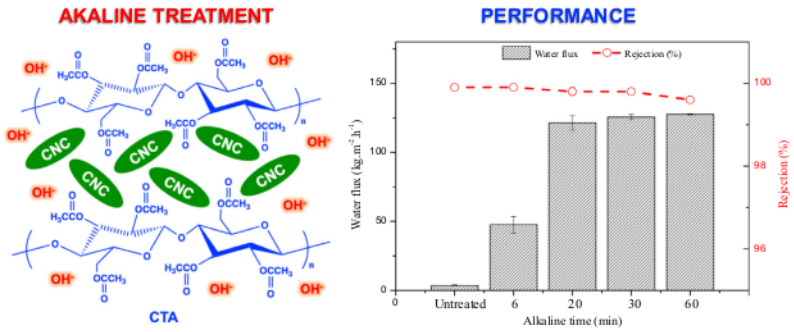

ARTICLE INFO

Article history:
Received 15 September 2020
Received in revised form 27 October 2020
Accepted 2 November 2020
Available online xxxx

Keywords:
Alkaline treatment
Hypersaline water
Pervaporation
Desalination
Cellulose nanocrystals

ABSTRACT

Cellulose triacetate/cellulose nanocrystals (CTA/CNCs) nanocomposite has recently been proposed as a promising material to synthesize pervaporation desalination membrane. However, the water flux of such membranes was found poor in comparison to other pervaporation desalination membranes. In this work, time-controlled alkaline treatment is proposed to improve the water flux of CTA/CNCs nanocomposite membrane without compromising its selectivity. An understanding how alkaline treatment changed the physicochemical properties of the membranes was obtained through membrane characterization by FTIR spectroscopy, X-ray diffraction, scanning electron microscopy (SEM), contact angle and water uptake analysis. The membrane being treated up to 30 min results in a drastic water flux improvement to 107.5 kg m^{-2} h^{-1} with >99.8% salt rejection in comparison with the water flux obtained by the untreated membrane, 3.6 kg m^{-2} h^{-1}, when hypersaline water with 90 g/L NaCl was employed as the feed solution. The water flux decreased to 58.5 kg m^{-2} h^{-1} when 200 g/L NaCl was used as feed solution. The alkali-treated membrane showed a stable membrane performance for 12 h when it was evaluated for 90 g/L and 200 g/L NaCl.

1. Introduction

Membrane-based desalination is a promising technology to augment fresh water supplies. Pressure-driven reverse osmosis (RO) is currently the forefront seawater desalination technology

* Corresponding authors at: Department of Chemical Engineering, KU Leuven, Celestijnenlaan 200F, B-3001 Leuven, Belgium.
E-mail addresses: indahprihatiningtyas.yamsidi@kuleuven.be (I. Prihatiningtyas), bart.vanderbruggen@kuleuven.be (B. Van der Bruggen).

https://doi.org/10.1016/j.ces.2020.116276
0009-2509/

due to the absence of a phase change during the separation process, making this technology highly energy efficient and cost-effective in providing potable water compared to thermal-based desalination processes (Gordon and Hui, 2016). The state-of-the-art RO membrane is a thin-film composite membrane, comprising a porous polymer support with a thin film of polyamide prepared via interfacial polymerization deposited on top of this support (Hartanto et al., 2020; Li et al., 2019b; Ali, 2019). The real game-changer has been the use of highly efficient pressure recovery systems for RO. However, this type of membrane is prone to fouling due to the intrinsic properties of polyamide materials. Furthermore, RO desalination has a limited water recovery and thus a large volume of brine is generated, which needs further treatment before being discharged to the environment (Lee et al., 2019). Although there has been an interest in applying high pressure reverse osmosis (HPRO) desalination to treat high salinity feed streams (Davenport et al., 2018), RO membranes have limited water recovery due to the very high osmotic pressure of the feed solution.

In recent years, alternative membrane-based desalination processes, such as hybrid processes making use of forward osmosis (FO), and membrane distillation (MD), have been studied as alternatives to RO desalination due to their excellent potential in handling high salinity streams. Unfortunately, FO requires much energy to re-concentrate the diluted draw solution (McGovern and Lienhard, 2014) while membrane wetting and a high fouling propensity are inherent drawbacks of MD (Lu et al., 2019). Pervaporation desalination is recently proposed as an emerging membrane desalination technology addressing several drawbacks of MD in dealing with high salinity streams. Instead of porous hydrophobic membranes, pervaporation desalination uses a dense hydrophilic membrane to perform desalination. The application of dense membranes results in a very high salt selectivity. The hydrophilic membrane surface also diminishes the fouling problems encountered in MD. However, the low membrane water permeability is a major hurdle for desalination by pervaporation (Liu, 2018).

Currently, there are two types of pervaporation desalination membranes: dense symmetric and thin-film composite (TFC) membranes. The former are prepared via solution casting followed by solvent evaporation, while the latter are usually prepared by interfacial polymerization or solution coating to deposit a highly selective salt rejection layer on top of a porous polymer support. Developing high performance membranes by improving the water transport rate inside the polymer matrix while maintaining a high salt selectivity is currently the major research focus in pervaporation desalination. One of the strategies to achieve this goal is to incorporate nanofillers inside the polymer matrix for dense or TFC membranes, to prepare nanocomposite membranes with improved water permeance. Various nanomaterials have been investigated to prepare nanocomposite membranes for pervaporation desalination applications, (Prihatiningtyas and Van Der Bruggen, 2020) such as SiO_2 (Talluri et al., 2020; Jullok, 2016; Chen et al., 2018), TiO_2 (Liu, 2019; Ataeivarjovi et al., 2019; Jhaveri et al., 2017), Al_2O_3 (Knozowska et al., 2020; Prihatiningtyas et al., 2020c); graphene oxide (GO) (Li et al., 2019a; Castro-Muñoz, 2019; Tang et al., 2019), and cellulose nanocrystals (Prihatiningtyas et al., 2019, 2020a). It has been showed that the incorporated nanofillers were able to significantly increase the water permeability due to the availability of additional water passages inside the polymer matrix. Furthermore, the mechanical properties of nanocomposite membranes are usually improved compared to their pristine version, considering that these membranes are usually very thin.

Cellulose nanocrystals are an emerging nanomaterial that has inherent hydrophilicity due to the presence of hydroxyl, sulfonic acid and carboxylic acid functional groups on its surface. It is one of the emerging nanofillers to prepare nanocomposite membranes for water desalination applications. In this work, alkali-treated cellulose triacetate/cellulose nanocrystal nanocomposite membranes were prepared and evaluated in desalination by pervaporation. The prepared membranes were systematically characterized to reveal the effect of alkaline treatment on membrane physicochemical properties and performance. Optimizing the alkaline treatment time of these nanocomposite membranes allowed to significantly enhance water flux without compromising the salt selectivity. The optimized membrane were applied to handle high salinity feed and had a stable performance during 12 h pervaporation experiments.

2. Experimental

2.1. Materials

Cellulose triacetate (CTA, acetyl content 43–44%, molecular weight 966.845 g/mol, Acros Organics TM) was used as the polymer matrix. Cellulose nanocrystals with an aggregated particle size of 1–50 μm, the diameter of 2.3–4.5 nm and the length of 44–108 nm as reported by the supplier, were obtained from CelluForce Inc. (Canada). Sodium chloride (NaCl) (99.5%) from Acros was employed as the solute in the feed solution. Sodium hydroxide (NaOH) was purchased from Fisher scientific, UK. All chemicals were used without further purification.

2.2. Membrane preparation

The CNCs suspensions were prepared by dispersing 3 wt% CNCs (calculated based on dope solution weight) in DMSO as a solvent. The suspension was mixed with a magnetic stirrer for three hours at 40 °C. Subsequently, 6 wt% CTA was loaded to the CNCs suspensions and the mixture was stirred for 15 h. The casting dope solution was left for an hour and was centrifuged for 4 min at 4000 rpm to remove bubbles generated from stirring process. The polymer films were prepared by casting the dope solution on the glass plate using an automatic casting device with a blade height of 200 μm at room temperature and a relative humidity of 34–44%. The wet polymer films were left in a vacuum oven for four hours at 60 °C and 0.17 bar to evaporate the solvent. The dried membranes were detached from the glass plate by immersing them into a water bath.

2.3. Alkaline treatment

A sodium hydroxide (NaOH) solution with a concentration of 2 M was prepared by dissolving in deionized water with a final pH of 13.25. Alkaline treatment of the membranes was conducted by immersing the membrane in the solution for different time periods, i.e., 6, 20, 30, and 60 min. The membranes were then directly evaluated in the pervaporation setup after the alkaline treatment. The detailed steps supplied with photos can be seen in Fig. S2.

2.4. Membrane characterization

2.4.1. Morphological characterization

The surface and cross-section morphologies of pristine and alkali-treated CTA/CNCs nanocomposite membrane were characterized using a scanning electron microscope (SEM) (Philips XL30 SEM, the Netherlands). For surface analysis of the pristine CTA/CNCs nanocomposite membrane with thickness 10 μm, the dried membrane samples were cut in small pieces, and then pasted on the SEM holder while the samples for cross-section analysis were

prepared by immersing the membranes in liquid nitrogen followed by fracturing the membranes before putting them onto the SEM holders. For sample preparation of alkali-treated membranes, the samples were cut with size 4 × 4 cm, then immersed in the 2 M NaOH solution at different times (6, 20, 30, and 60 min). Then the samples were immersed in DI water for 30 s to remove the remaining NaOH solution on the membrane. The treated membrane was directly cut into small pieces and pasted on the SEM holder for surface characterization. For cross-section characterization, the treated membranes were immersed in liquid nitrogen and fractured before pasting them onto the SEM holder.

2.4.2. X-ray diffraction (XRD)

X-ray diffraction analysis was employed to probe the structural changes of CTA/CNCs nanocomposite membranes after the alkaline treatment. X-ray diffraction model Philips PW1830 diffractometer was used with Bragg/Brentano θ–2θ setup, CuKα radiation at 45 kV – 30 mA on 173 mm goniometer circle, within the scan range of 3–75°(Rietveld users), for 1 h.

2.4.3. FTIR analysis

The chemical composition of the untreated CTA/CNCs nanocomposite membrane and alkali-treated membranes was characterized using attenuated total reflectance-Fourier transform infrared spectroscopy (ATR-FTIR, Perkin Elmer, spectrum 100, USA). At least 4 scanning for each sample were conducted in the span range of 4000–650 cm^{-1}.

2.4.4. Water uptake measurement

Water uptake measurement was conducted to study the effect of alkaline treatment on the swelling properties of the nanocomposite membranes. The membranes were cut into a diameter of 6 cm and were immersed in DI water at room temperature for two days to reach equilibrium condition. The wet membranes were wiped with a tissue to remove unabsorbed water before weighing to obtain the mass of wet membranes (M_w). Next, the membranes were dried in the oven at 105 °C for one day to evaporate the adsorbed water and were weighed to obtain the mass of dried membrane (M_d). Triplicate measurements were done for each membrane to ensure accuracy. The water uptake of the membranes was calculated according to the following equation.

$$Water\ uptake\ (\%) = \frac{M_w - M_d}{M_d} \times 100\% \quad (1)$$

2.4.5. Pervaporation experiment

The performance of CTA/CNCs nanocomposite membranes (pristine and alkali-treated membranes) for pervaporation desalination was evaluated using a laboratory scale setup shown schematically in Fig. 1. A feed solution was prepared by dissolving NaCl in water and poured into the feed tank. The feed solution was then heated until a predetermined operating temperature was reached. The liquid feed was circulated with a peristaltic pump into the membrane module (membrane area was 19.625 cm^2) with a flow rate of 70–80 L/h. A vacuum pump with low pressure (below 1 mbar) was employed on the permeate side to generate vapor pressure difference across the membrane. The permeating vapor was collected and condensed with a double U glass tube immersed in liquid nitrogen acting as the cold trap. The collected permeate was weighed during 3 h pervaporation process.

The water flux, J ($kg\ m^{-2}\ h^{-1}$) and salt rejection, R (%) of the pervaporation membranes were calculated using the following equations:

$$Water\ flux(J) = \frac{m}{(Axt)} \quad (2)$$

$$Rejection\ (\%) = \frac{(Cf - Cp)}{Cf} \times 100\% \quad (3)$$

where m is the mass of the collected permeate (kg), A is the effective membrane area (m^2), t is the time period required to collect a certain amount of permeate (h), C_f is the salinity in the feed side and Cp is salinity the permeate solution. The salinity value was determined by a conductivity meter model Consort-C831.

3. Results and discussion

3.1. Membrane characterization

3.1.1. Morphological characterization

The SEM images displaying the surface structure of the untreated and alkali-treated CTA/CNCs pervaporation membrane are shown in Fig. S3. The figures show that the pristine as well as the alkali-treated nanocomposite membranes have a dense structure. The digital images of CTA/CNCs nanocomposite untreated and alkali-treated are shown in Fig. S1. Fig S1a shows that the untreated CTA/CNCs nanocomposite is dry and rigid while Fig. S1b shows that CTA/CNCs membrane after 30 min treatment in 2 M of solution NaOH was wet and soft.

The alkaline treatment also affects the cross-section morphology of the CTA/CNCs nanocomposite membrane, as shown in Fig. 2. Fig. S5a shows that the membrane floated on the NaOH solution. However, the membrane was slightly drowned in the solution after 20 min immersion (see Fig. S5b), hence the alkali process is not only occurring on the membrane surface but also in the membrane cross section. Fig. 2a shows that the cross-section of the

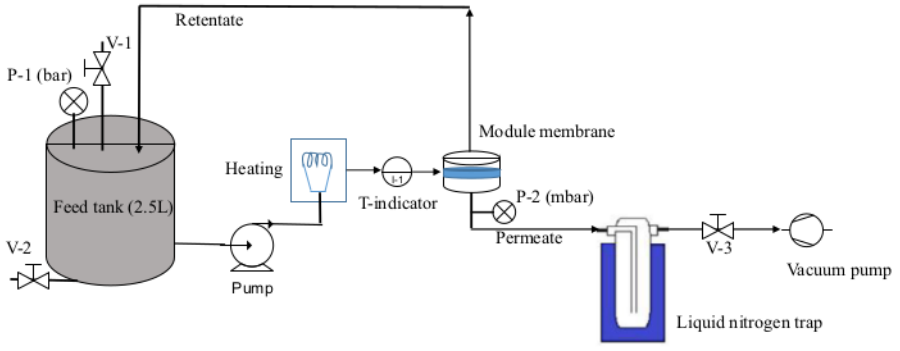

Fig. 1. Schematic flow chart of laboratory scale for pervaporation desalination.

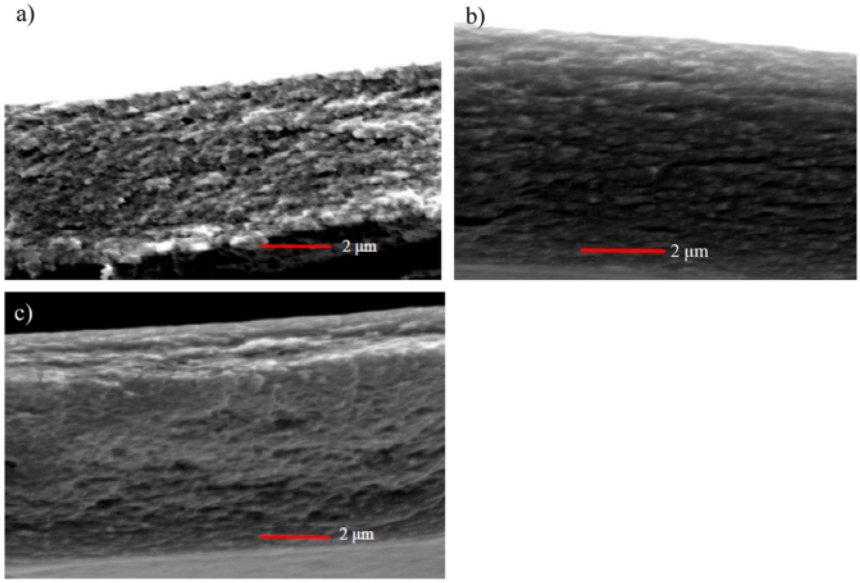

Fig. 2. SEM images of membrane cross-section: (a) Untreated, (b) 20 min of alkaline treatment, and (c) 30 min of alkaline treatment.

untreated membrane has a layered porous structure. The cross-section structure seems denser after 20 min of alkaline treatment (see Fig. 2b); the structure more compact and dense after being treated in alkaline environment for 30 min (see Fig. 2c). After 30 min in alkali solution, the membrane pores also appear to be collapsed due to the deacetylation process, which is in agreement with the literature (Wittmar et al., 2015).

3.1.2. X-ray diffraction D

Fig. 3 describes the X-ray diffraction results of the CTA/CNCs nanocomposite membrane at different times of alkaline treatment. The characteristic peaks of cellulose generally appear around 15°, 22°, and 35° (Malucelli et al., 2020). The XRD spectrum for the untreated film membrane, as shown in Fig. 3a, indicates the characteristic peak of cellulose triacetate around 5–10° due to acetylation of cellulose (Malucelli et al., 2020). However, these peaks disappear for the alkali-treated CTA/CNCs membrane (see Fig. 3b–e). The crystalline structure of CTA/CNCs membrane was investigated based on the commonly used crystalline peak of cellulose, i.e., around 22°. Fig. 3b depicts that the crystalline structure of the CTA/CNCs nanocomposite membrane decreased after being alkali-treated for 6 min. However, an increasing alkaline treatment time, starting at 20 min, increases the crystalline structure of the membrane again (see Fig. 3c–e). This increase might be due to the cellulose recrystallization (Bali et al., 2015). Alkaline treatment is able to enhance the crystal size and crystalline index of cellulose (Xu et al., 2020; Chieng et al., 2017) due to the removal of lignin (Chieng et al., 2017). Furthermore, Santos et al. reported that alkaline treatment with NaOH in hot water at 75 °C enhanced the crystalline index of the piassava fibers with a decrease of the amorphous phase (Santos, 2018).

3.1.3. FTIR characterization

FTIR spectra of the untreated and alkali-treated of CTA/CNCs nanocomposite membranes are shown in Fig. 4. The functional groups in Fig. 4a appear as a peak at 3328 cm^{-1} referring to O—H stretching, while the peak at 2891 cm^{-1} relates to the stretching of aliphatic C—H bonds. Fig. 4b shows the bands at 1744 cm^{-1}, 1643 cm^{-1}, and 1365 cm^{-1} attributed to the C=O stretching, the C=C stretching, and the asymmetric bending of C=H, respectively

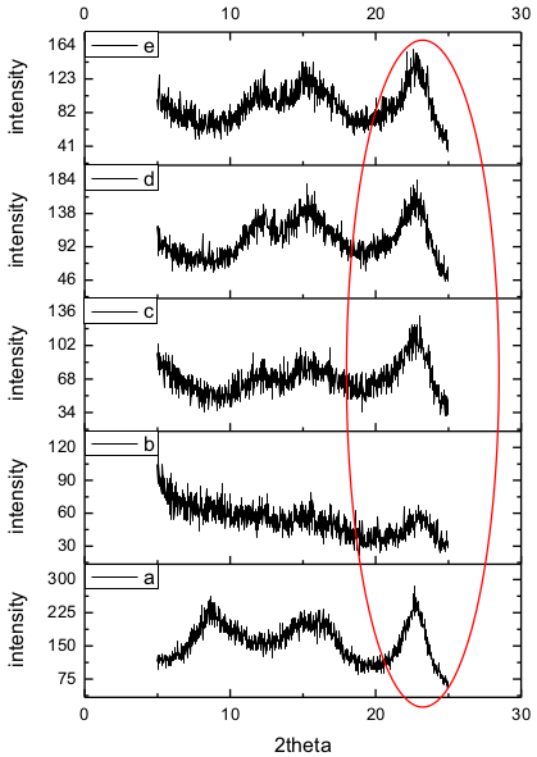

Fig. 3. X-ray diffraction at different times of alkaline treatment: (a) Untreated, (b) 6 min, (c) 20 min, (d) 30 min, and (d) 60 min.

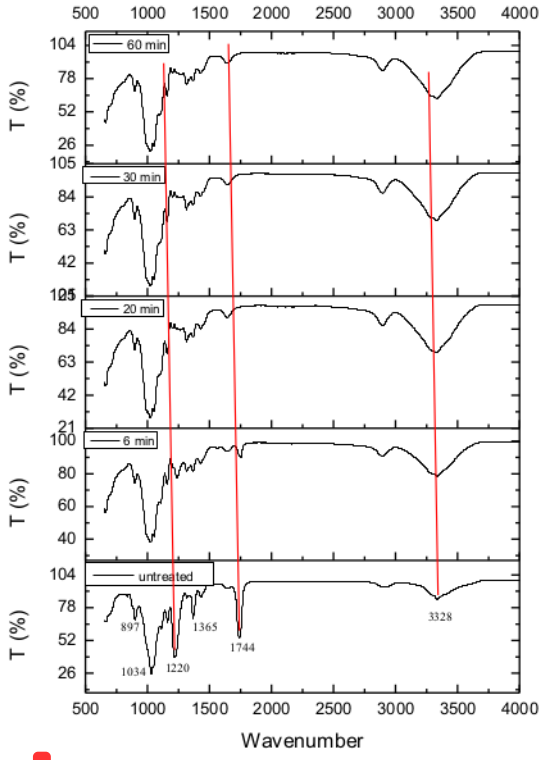

Fig. 4. FTIR spectra of CTA/CNCs nanocomposite membranes at different time of alkaline treatment, (a) Wavenumber range in 2000–4000 cm^{-1}, (b) Wavenumber range in 600–2200 cm^{-1}.

(Prihatiningtyas et al., 2019; Santos, 2018). The peaks at 1220 cm^{-1} and 1034 cm^{-1} correspond to C—O stretching and the pyranose ring C—O—C (Prihatiningtyas et al., 2019), while the band at 897 cm^{-1} is corresponding to the β-glycosidic linkages of the glucose ring, which it is a typical structure of cellulose (Chieng et al., 2017; Santos, 2018). The spectrum after alkaline treatment as presented in Fig. 4a suggests that the peak intensity at 3328 cm^{-1} has an increasing trend. This trend indicates the enhancement of O—H groups due to the deacetylation process, as shown in Fig. 5, which substitutes the acetate groups with the hydroxyl groups. The enhancement of O-H groups shows that the hydrophilicity of the CTA/CNCs nanocomposite membrane increased after alkaline treatment. However, the peak at 1220 cm^{-1} (C—O) and 1744 cm^{-1} (C=O) decreased and almost disappeared after alkaline treatment due to acetate elimination.

3.1.4. Water uptake measurement

Water uptake was measured to investigate the effect of alkaline treatment on the water absorption of the CTA/CNCs nanocomposite membrane. Fig. 6 reveals that alkaline treatment of the CTA/CNCs nanocomposite membrane significantly enhances the absorption of water. Fig. 6 shows that water uptake increased drastically by 421% after 6 min of alkaline treatment compared to the untreated membrane. A further increase of the alkaline treatment time to 20, 30 and 60 min only increased the water uptake by 36%, 24% and 13%, respectively. The large improvement of water uptake indicates that the alkaline treatment has a positive impact on altering the hydrophilicity of the CTA/CNCs nanocomposite membrane. Longer alkaline treatment times resulted in an increasing water uptake of the nanocomposite membranes. This is also confirmed by FTIR results, as shown in Fig. 4: an increasing time of alkaline treatment enhances the O-H groups, which leads to an improvement of membrane hydrophilicity.

3.1.5. Contact angle

The increase of membrane surface hydrophilicity after the alkaline treatment was also characterized by contact angle measurement. Fig. 7 shows that the membrane contact angle decreased from 65.6° to 26.3° after only 6 min of alkaline treatment. On the other hand, there was no significant decrease in contact angle when the alkaline time was increased from 6 to 30 min (26.3° to 24.7°). The decreasing contact angle to 26.27° and 24.7° indicates that alkaline treatment is a very effective method to enhance the surface hydrophilicity of the CTA/CNCs nanocomposite membranes.

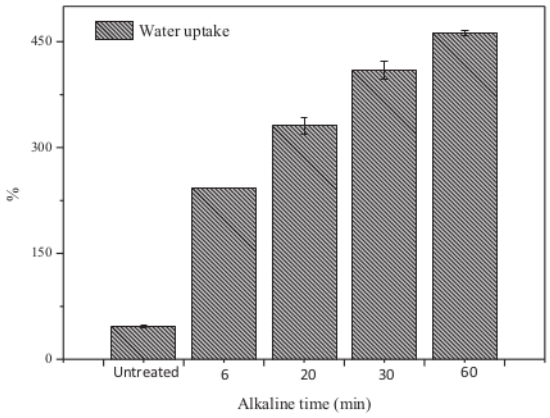

Fig. 6. Water uptake the membranes at different time of alkaline treatment.

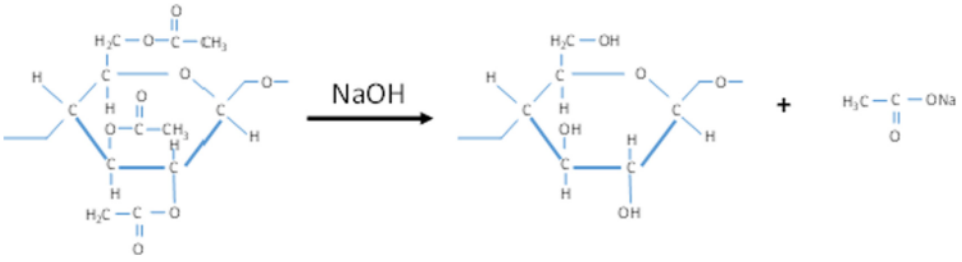

Fig. 5. Deacetylation of cellulose triacetate with NaOH.

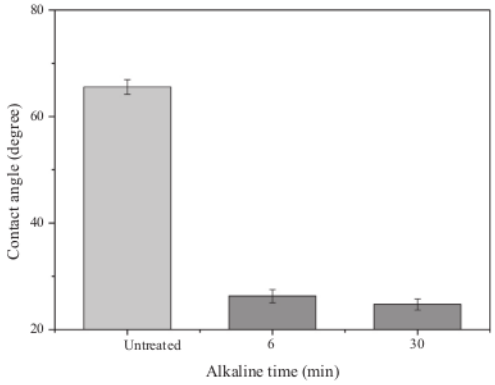

Fig. 7. Contact angle at different time of alkaline treatment.

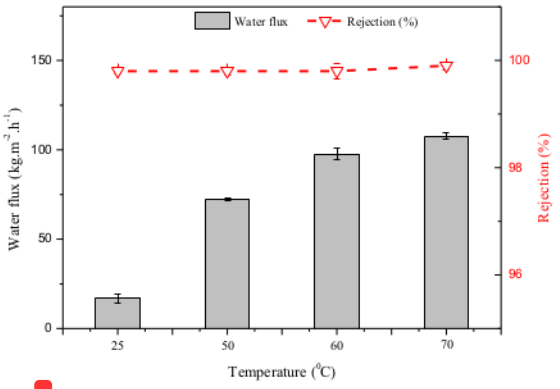

Fig. 9. Pervaporation performance of CTA/CNCs nanocomposite membrane (30 min in alkali treatment) at different temperatures.

3.2. Performance of CTA/CNCs nanocomposite membranes in PV desalination

3.2.1. Effect of time of alkaline treatment on membrane performance

The influence of the alkaline treatment time on the pervaporation performance of the CTA/CNCs nanocomposite membranes in desalination is shown in Fig. 8. The water flux of the nanocomposite membranes can be significantly improved by simply controlling the alkaline treatment period. The water flux enhanced from 3.6 kg m^{-2} h^{-1} to 24 kg m^{-2} h^{-1} (567%) when the CTA/CNCs nanocomposite membrane was treated in NaOH solution for 6 min with an intact salt rejection, maintaining at 99.9%. The water flux was further increased by 347%, from 24 kg m^{-2} h^{-1} to 107.5 kg m^{-2} h^{-1}, when the alkaline treatment was prolonged from 6 min to 30 min with salt rejection kept of 99.9%. This considerable water flux increase can be attributed to the increase of the membrane hydrophilicity, as evidenced by water uptake measurements and the increase in hydrophilic functional groups measured by FTIR. This, in turn, will enhance the mass transport rate of water molecules inside nanocomposite membranes during pervaporation. Increasing the alkaline treatment time beyond 30 min had a very small effect on the water flux. In fact, a decreasing salt selectivity was observed when 60 min alkaline treatment time was employed. This remarkable flux and salt selectivity can be attributed to the dense structure of the membrane surface after the alkaline treatment with improved hydrophilic character of the membranes.

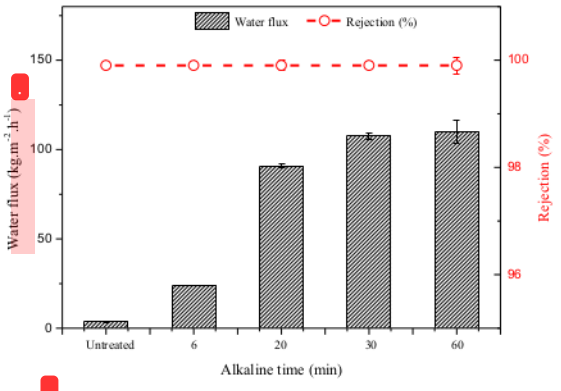

Fig. 8. Pervaporation performance of CTA/CNCs nanocomposite membrane at different times of alkaline treatment.

3.2.2. Effect of feed temperature on membrane performance

The effect of feed temperature on the pervaporation performance was investigated in the range 25–70 °C, as shown in Fig. 9. It can be seen that rising the feed temperature from 25 to 70 °C results in an increase of water flux from 16 kg m^{-2} h^{-1} to 107.5 kg m^{-2} h^{-1} without significantly compromising the membrane salt selectivity as the salt rejection was maintained at 99.9%. The increasing water flux is not surprising; the driving force in pervaporation process is the difference of partial pressure between the feed and permeate side, as predicted by the Antoine equation (Lawal and Khalifa, 2014). As the partial pressure of the permeate side is held constant, changing the partial pressure at the feed side will lead to a change in driving force (Xie et al., 2011). Furthermore, a higher temperature results in a higher water diffusivity (Svang-Ariyaskul, 2006), leading to a faster water transport rate inside the membranes.

Theoretically, the relationship of water flux with operating temperature can be explained by the Arrhenius equation (Yeom and Lee, 1997; Jiraratananon et al., 2002; Peng et al., 2006).

$$J_i = J_o \exp\left(-\frac{E_{p,i}}{RT}\right) \quad (4)$$

where J_i is the water flux of i, J_o is the pre-exponential factor, R is the gas constant, T is the absolute temperature and $E_{p,i}$ is the apparent activation energy for permeation. Fig. 10 depicts the Arrhenius correlation, which shows the logarithmic relation between the water fluxes and the reciprocal operating temperatures. The water activation energy is 37.8 kJ mol^{-1}; the positive value of the activation energy indicates that the water flux enhances with temperature at the feed side (Kittur et al., 2003).

3.2.3. Performance of CTA/CNCs at different feed concentrations

Fig. 11 shows the effect of the NaCl concentration in the feed solution on the pervaporation performance. It can be seen that adding 90 g/L of NaCl in the pure water feed solution decreases the water flux by 31.5%, from 157 k m^{-2} h^{-1} to 107.5 k m^{-2} h^{-1}. While increasing NaCl concentration from 90 g/L to 200 g/L decreases the water flux. Decreases the water flux by 45.5% from 107.5 k m^{-2} h^{-1} to 58.5 kg m^{-2} h^{-1}, however, the salt rejection is still kept at 99.9%. It has been reported in the literature that the feed concentration directly affects the sorption of the species at the membrane surface (Jiraratananon et al., 2002). Increasing the NaCl concentration from 9 wt% to 20 wt% corresponds to a reduction of the water concentration from 91 wt% to 80 wt%, which

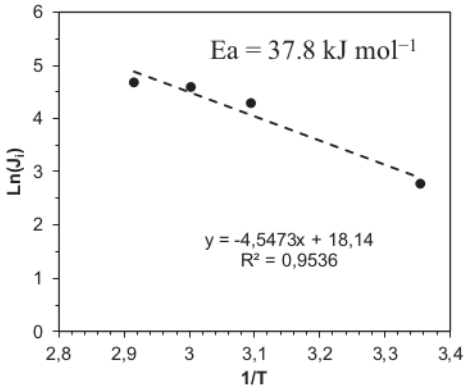

Fig. 10. Arrhenius plot of ln (Ji) and 1000/T of CTA/CNCs nanocomposite membrane (30 min in alkaline treatment).

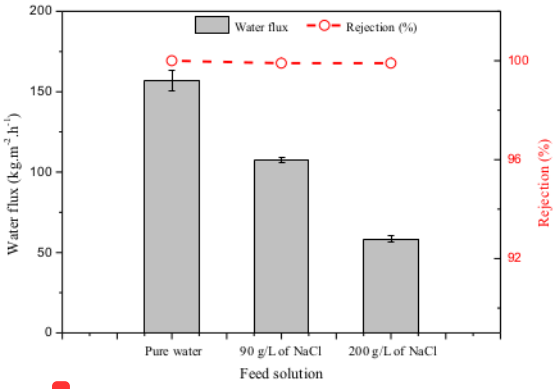

Fig. 11. Pervaporation performance of CTA/CNCs nanocomposite membrane (30 min in alkali treatment) at different NaCl concentrations.

subsequently reduces the sorption of water molecules at the membrane interface (Wu et al., 2018). This causes the water diffusion crossing the membrane to decrease, leading to a reduction in the water flux. As 30 min alkaline treatment resulted in optimized membrane performance, this membrane was further evaluated for 12 h pervaporation desalination with 90 g/L and 200 g/L of NaCl as the feed solutions. Fig. 12 reveals that a stable membrane water flux can be obtained with a stable salt rejection in the range of 99.8–99.9%. Subsequently, this promising membrane performance will be suitable to treat feed solutions with hypersaline conditions.

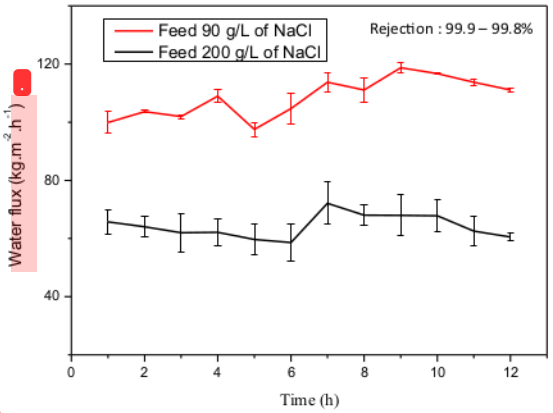

Fig. 12. Pervaporation performance of CTA/CNCs nanocomposite membrane (30 min in alkali treatment) at different NaCl concentrations during 12 h pervaporation process.

Driving force for pervaporation desalination relies on the chemical potential gradient between the feed side and permeate side of the membrane (Slater et al., 2006; Cannilla et al., 2017) which the concentration gradient could be expressed in terms of partial pressure (Franken et al., 1990). Currently, pervaporation is a growing interest in applying to treat hypersaline feeds. Table 1 compares the recently developed pervaporation membranes for hypersaline feed conditions.

4. Conclusion

Alkaline treatment of a CTA/CNCs nanocomposite membrane results in an enhancement of the pervaporation desalination performance. Alkaline treatment does not significantly change the membrane surface morphology. Hence, the salt rejection is still maintained above 99%. Alkaline treatment generates a gelation process on the membrane and improves the hydrophilicity, which leads to an increased water flux. The optimum time of alkaline treatment is 30 min at operating temperature of 70 °C with an increase of water flux from 3.6 kg m^{-2} h^{-1} to 107.5 kg m^{-2} h^{-1} for a feed solution of 90 g/L NaCl. For 200 g/L of NaCl in the feed solution, the water flux is 58.5 kg m^{-2} h^{-1}. Alkaline treatment of the CTA/CNCs nanocomposite membrane allows to maintain a high salt rejection, above 99.8%, at hypersaline feed conditions. This

Table 1
Summary of the recently developed pervaporation desalination membranes.

Membranes	Feed concentration (g/L)	Operating temperature (°C)	Flux (kg m^{-2} h^{-1})	Rejection (%)	Ref.
CTA/CNCs	90	70	7.6	99.7	(Prihatiningtyas et al., 2020a)
CTA/Al_2O_3	90	70	5.0	99.8	(Prihatiningtyas et al., 2020c)
CTA/Ludox-SiO_2	60	70	4.8	99.8	(Prihatiningtyas et al., 2020b)
sPEEK/PES	100	70	4.9	>99.97	(Zeng, 2020)
PA/GO	100	70	24	99.99	(Zhao et al., Jul. 2020)
MAX-MXene	35	30	22.8	>99.7	(Ding, 2020)
GO-PVA	100	85	98.0	99.99	(Sun et al., 2020)
PVA/P(AA-AMPS)	200	75	74.1	99.7	(Xue et al., 2020)
PVA/silicate nanoclay	100	40	21.1	~99.99	(Selim et al., 2020)
LbL PEI/GO	200	65	8.4	99.9	(Halakoo and Feng, 2020)
PVA/GA/Laponite	100	70	39.9	99.9	(Selim, 2019)
Alkali treated CTA/CNCs	90	70	107.5	>99.8	This work
	200	70	58.5	>99.8	This work

work shows that a simple alkaline treatment of CTA/CNCs nanocomposite membranes can be a tool to enhance the performance of this class of pervaporation desalination membranes with a promising capability to treat hypersaline feed solutions in a very efficient way.

CRediT authorship contribution statement

Indah Prihatiningtyas: Conceptualization, Methodology, Formal analysis, Investigation, Writing - original draft, Writing - review & editing, Visualization. **Yusak Hartanto:** Formal analysis, Writing - review & editing, Visualization. **Bart Van der Bruggen:** Writing - review & editing, Supervision, Project administration.

Declaration of Competing Interest

The authors declare that they have no known competing financial interests or personal relationships that could have appeared to influence the work reported in this paper.

Acknowledgment

This research was supported by the Indonesia Endowment Fund for Education (LPDP). The authors would like to thank to Chritine wouters (KU Leuven) for measuring FTIR.

Appendix A. Supplementary material

Supplementary data to this article can be found online at https://doi.org/10.1016/j.ces.2020.116276.

References

Ali, Z. et al., 2019. Defect-free highly selective polyamide thin-film composite membranes for desalination and boron removal. J. Memb. Sci. 578, 85–94.
Ataeivarjovi, E., Tang, Z., Chen, J., Zhao, Z., Dong, G., 2019. Enhancement of CO2 desorption from a novel absorbent (dimethyl carbonate) by using a PDMS/TiO2 pervaporation membrane. ACS Sustain. Chem. Eng. 7 (14), 12125–12137.
Bali, G., Meng, X., Deneff, J.I., Sun, Q., Ragauskas, A.J., 2015. The effect of alkaline pretreatment methods on cellulose structure and accessibility. ChemSusChem 8 (2), 275–279.
Cannilla, C., Bonura, G., Frusteri, F., 2017. Potential of pervaporation and vapor separation with water selective membranes for an optimized production of biofuels—a review. Catalysts 7 (6).
Castro-Muñoz, R. et al., 2019. Towards the dehydration of ethanol using pervaporation cross-linked poly(vinyl alcohol)/graphene oxide membranes. J. Memb. Sci. 582, 423–434.
Chen, K.-F., Zheng, P.-Y., Wu, J.-K., Wang, N.-X., An, Q.-F., Lee, K.-R., 2018. Polyelectrolyte complexes/silica hybrid hollow fiber membrane for fusel oils pervaporation dehydration processes. J. Memb. Sci. 545, 284–291.
Chieng, B.W., Lee, S.H., Ibrahim, N.A., Then, Y.Y., Loo, Y.Y., 2017. Isolation and characterization of cellulose nanocrystals from oil palm mesocarp fiber. Polymers (Basel) 9 (8), 1–11.
Davenport, D.M., Deshmukh, A., Werber, J.R., Elimelech, M., 2018. High-pressure reverse osmosis for energy-efficient hypersaline brine desalination: current status, design considerations, and research needs. Environ. Sci. Technol. Lett. 5 (8), 467–475.
Ding, M. et al., 2020. 2D laminar maleic acid-crosslinked MXene membrane with tunable nanochannels for efficient and stable pervaporation desalination. J. Memb. Sci. 600, 117871.
Franken, A.C.M., Mulder, M.H.V., Smolders, C.A., 1990. Pervaporation process using a thermal gradient as the driving force. J. Memb. Sci. 53 (1–2), 127–141.
Gordon, J.M., Hui, T.C., 2016. Thermodynamic perspective for the specific energy consumption of seawater desalination. Desalination 386, 13–18.
Halakoo, E., Feng, X., 2020. Layer-by-layer assembly of polyethyleneimine/graphene oxide membranes for desalination of high-salinity water via pervaporation. Sep. Purif. Technol. 234, 116077.
Hartanto, Y., Corvilain, M., Mariën, H., Janssen, J., Vankelecom, I.F.J., 2020. Interfacial polymerization of thin-film composite forward osmosis membranes using ionic liquids as organic reagent phase. J. Memb. Sci. 601, 117869.
Jhaveri, J.H., Patel, C.M., Murthy, Z.V.P., 2017. Preparation, characterization and application of GO-TiO2/PVC mixed matrix membranes for improvement in performance. J. Ind. Eng. Chem. 52, 138–146.
Jiraratananon, R., Chanachai, A., Huang, R.Y.M., Uttapap, D., 2002. Pervaporation dehydration of ethanol–water mixtures with chitosan/hydroxyethylcellulose (CS/HEC) composite membranes: I. Effect of operating conditions. J. Memb. Sci. 195 (2), 143–151.
Jullok, N. et al., 2016. Effect of silica nanoparticles in mixed matrix membranes for pervaporation dehydration of acetic acid aqueous solution: plant-inspired dewatering systems. J. Clean. Prod. 112, 4879–4889.
Kittur, A.A., Karidurаganavar, M.Y., Toti, U.S., Ramesh, K., Aminabhavi, T.M., 2003. Pervaporation separation of water–isopropanol mixtures using ZSM-5 zeolite incorporated poly(vinyl alcohol) membranes. J. Appl. Polym. Sci. 90 (9), 2441–2448.
Knozowska, K., Li, G., Kujawski, W., Kujawa, J., 2020. Novel heterogeneous membranes for enhanced separation in organic-organic pervaporation. J. Memb. Sci. 599, 117814.
Lawal, D.U., Khalifa, A.E., 2014. Flux prediction in direct contact membrane distillation. Int. J. Mater. Mech. Manuf. 2 (4), 302–308.
Lee, S., Choi, J., Park, Y.-G., Shon, H., Ahn, C.H., Kim, S.-H., 2019. Hybrid desalination processes for beneficial use of reverse osmosis brine: current status and future prospects. Desalination 454, 104–111.
Li, L., Hou, J., Chen, V., 2019a. Pinning down the water transport mechanism in graphene oxide pervaporation desalination membranes. Ind. Eng. Chem. Res. 58 (10), 4231–4239.
Li, Y., Wong, E., Mai, Z., Van der Bruggen, B., 2019b. Fabrication of composite polyamide/Kevlar aramid nanofiber nanofiltration membranes with high permselectivity in water desalination. J. Memb. Sci. 592, 117396.
Liu, G. et al., 2018. Ultrathin two-dimensional MXene membrane for pervaporation desalination. J. Memb. Sci. 548, 548–558.
Liu, X.-W. et al., 2019. High-performance polyamide/ceramic hollow fiber TFC membranes with TiO2 interlayer for pervaporation dehydration of isopropanol solution. J. Memb. Sci. 576, 26–35.
Lu, K.J., Chen, Y., Chung, T.-S., 2019. Design of omniphobic interfaces for membrane distillation – a review. Water Res. 162, 64–77.
Malucelli, L.C., Lomonaco, D., Filho, M.A.S.C., Magalhães, W.L.E., 2020. Cellulose triacetate from different sources: modification assessment through thermal and chemical characterization. Holzforschung 74 (5), 505–512.
McGovern, R.K., Lienhard, J.H.V., 2014. On the potential of forward osmosis to energetically outperform reverse osmosis desalination. J. Memb. Sci. 469, 245–250.
Peng, F., Lu, L., Sun, H., Jiang, Z., 2006. Analysis of annealing effect on pervaporation properties of PVA-GPTMS hybrid membranes through PALS. J. Memb. Sci. 281 (1), 600–608.
Prihatiningtyas, I., Volodin, A., Van Der Bruggen, B., 2019. 110th anniversary: cellulose nanocrystals as organic nanofillers for cellulose triacetate membranes used for desalination by pervaporation. Ind. Eng. Chem. Res. 58 (31), 14340–14349.
Prihatiningtyas, I., Li, Y., Hartanto, Y., Vananroye, A., Coenen, N., Van der Bruggen, B., 2020a. Effect of solvent on the morphology and performance of cellulose triacetate membrane/cellulose nanocrystal nanocomposite pervaporation desalination membranes. Chem. Eng. J. 388.
Prihatiningtyas, I., Hartanto, Y., Ballesteros, M.S.R., Van der Bruggen, B., 2020b. Cellulose triacetate/LUDOX-SiO 2 nanocomposite for synthesis of pervaporation desalination membranes. J. Appl. Polym. Sci. (September), 50000
Prihatiningtyas, I., Gebreslase, G.A., Van der Bruggen, B., 2020c. Incorporation of Al2O3 into cellulose triacetate membranes to enhance the performance of pervaporation for desalination of hypersaline solutions. Desalination 474, 114198.
Prihatiningtyas, I., Van Der Bruggen, B., 2020. Nanocomposite pervaporation membrane for. Chem. Eng. Res. Des. 164, 147–161.
Santos, E.B.C. et al., 2018. Effect of alkaline and hot water treatments on the structure and morphology of piassava fibers. Mater. Res. 21 (2), 1–11.
Selim, A. et al., 2019. Preparation and characterization of PVA/GA/Laponite membranes to enhance pervaporation desalination performance. Sep. Purif. Technol. 221, 201–210.
Selim, M.A., Toth, A.J., Fozer, D., Haaz, E., Mizsey, P., 2020. Pervaporative desalination of concentrated brine solution employing crosslinked PVA/silicate nanoclay membranes. Chem. Eng. Res. Des. 155, 229–238.
Slater, C.S., Schurmann, T., MacMillian, J., Zimarowski, A., 2006. Separation of diacteone alcohol-water mixtures by membrane pervaporation. Sep. Sci. Technol. 41 (12), 2733–2753.
Sun, J., Qian, X., Wang, Z., Zeng, F., Bai, H., Li, N., 2020. Tailoring the microstructure of poly(vinyl alcohol)-intercalated graphene oxide membranes for enhanced desalination performance of high-salinity water by pervaporation. J. Memb. Sci. 599, 117838.
Svang-Ariyaskul, A. et al., 2006. Blended chitosan and polyvinyl alcohol membranes for the pervaporation dehydration of isopropanol. J. Memb. Sci. 280 (1), 815–823.
Talluri, V.S.S.L.P., Tleuova, A., Hosseini, S., Vopicka, O., 2020. Selective separation of 1-butanol from aqueous solution through pervaporation using PTSMP-silica nano hybrid membrane. Membranes (Basel) 10 (4).
Tang, W., Lou, H., Li, Y., Kong, X., Wu, Y., Gu, X., 2019. Ionic liquid modified graphene oxide-PEBA mixed matrix membrane for pervaporation of butanol aqueous solutions. J. Memb. Sci. 581, 93–104.
Wittmar, A., Thierfeld, H., Köcher, S., Ulbricht, M., 2015. Routes towards catalytically active TiO2 doped porous cellulose. RSC Adv. 5 (45), 35866–35873.

Wu, D., Gao, A., Zhao, H., Feng, X., 2018. Pervaporative desalination of high-salinity water. Chem. Eng. Res. Des. 136, 154–164.

Xie, Z., Ng, D., Hoang, M., Duong, T., Gray, S., 2011. Separation of aqueous salt solution by pervaporation through hybrid organic-inorganic membrane: effect of operating conditions. Desalination 273 (1), 220–225.

Xu, E., Wang, D., Lin, L., 2020. Chemical structure and mechanical properties of wood cellwalls treated with acid and alkali solution. Forests 11 (1).

Xue, Y.L., Huang, J., Lau, C.H., Cao, B., Li, P., 2020. Tailoring the molecular structure of crosslinked polymers for pervaporation desalination. Nat. Commun. 11 (1).

Yeom, C.K., Lee, K.-H., 1997. Vapor permeation of ethanol-water mixtures using sodium alginate membranes with crosslinking gradient structure. J. Memb. Sci. 135 (2), 225–235.

Zeng, H. et al., 2020. Hydrophilic SPEEK/PES composite membrane for pervaporation desalination. Sep. Purif. Technol. 250, 117265.

Zhao, X., Tong, Z., Liu, X., Wang, J., Zhang, B., 2020. Facile preparation of polyamide-graphene oxide composite membranes for upgrading pervaporation desalination performances of hypersaline solutions. Ind. Eng. Chem. Res. 59 (26), 12232–12238.

Ultra-high flux alkali-treated cellulose triacetate/cellulose nanocrystal nanocomposite membrane for pervaporation desalination

ORIGINALITY REPORT

14%	0%	15%	2%
SIMILARITY INDEX	INTERNET SOURCES	PUBLICATIONS	STUDENT PAPERS

MATCH ALL SOURCES (ONLY SELECTED SOURCE PRINTED)

13%

★ Indah Prihatiningtyas, Yi Li, Yusak Hartanto, Anja Vananroye, Nico Coenen, Bart Van der Bruggen. "Effect of solvent on the morphology and performance of cellulose triacetate membrane/cellulose nanocrystal nanocomposite pervaporation desalination membranes", Chemical Engineering Journal, 2020

Publication

Exclude quotes	On	Exclude matches	< 2%
Exclude bibliography	On		